Two-photon image correlation spectroscopy and image cross-correlation spectroscopy

P. W. WISEMAN*, J. A. SQUIER†, M. H. ELLISMAN‡ & K. R. WILSON*

*Department of Chemistry & Biochemistry, University of California, San Diego, La Jolla, CA 92093-0339, U.S.A.

†Department of Electrical & Computer Engineering University of California, San Diego, La Jolla, CA 92093-0339, U.S.A.

‡National Center for Microscopy & Imaging Research (NCMIR), Department of Neurosciences, University of California, San Diego, La Jolla, CA 92093-0608, U.S.A.

Summary

We introduce two-photon image correlation spectroscopy (ICS) using a video rate capable multiphoton microscope. We demonstrate how video rate two-photon microscopic imaging and image correlation analysis may be combined to measure molecular transport properties over ranges typical of biomolecules in membrane environments. Using two-photon ICS, we measured diffusion coefficients as large as 10^{-8} cm^2 s^{-1} that matched theoretical predictions for samples of fluorescent microspheres suspended in aqueous sucrose solutions. We also show the sensitivity of the method for measuring microscopic flow using analogous test samples. We demonstrate explicitly the advantages of the image correlation approach for measurement of correlation functions with high signal-to-noise in relatively short time periods and discuss situations when these methods represent improvements over non-imaging fluorescence correlation spectroscopy. We present the first demonstration of two-photon image cross-correlation spectroscopy where we simultaneously excite (via two-photon absorption) non-identical fluorophores with a single pulsed laser. We also demonstrate cellular application of two-photon ICS for measurements of slow diffusion of green fluorescent protein/adhesion receptor constructs within the basal membrane of live CHO fibroblast cells.

Introduction

Fluorescence correlation spectroscopy (FCS) was originally developed as a microscopy method suited for measuring macromolecular transport properties and concentrations via autocorrelation analysis of the amplitude and temporal characteristics of fluorescence signals arising from spontaneous fluctuations in molecular occupation number within the system (Magde *et al.*, 1972; Elson & Magde, 1974; Magde *et al.*, 1974). The FCS technique uses a microscope objective lens to focus an input laser beam into a sample to define a diffraction limited, open excitation volume from which fluorescence photons may be collected as a function of time. The time variation in collected photon counts directly reflects fluctuations in the concentration of fluorophore molecules within the beam defined observation volume. More recently, other researchers have introduced a variety of extensions of the basic FCS method including the use of confocal pinholes to permit single molecular detection (Rigler *et al.*, 1993), two-photon excitation FCS for intracellular applications (Berland *et al.*, 1995), as well as dual colour fluorescence cross-correlation spectroscopy (Schwille *et al.*, 1997). These developments and recent applications of the technique for studies within living cells (Brock & Jovin, 1998; Schwille *et al.*, 1999) have led to a renewal of interest in FCS, especially for biological applications.

In addition to providing information on the molecular transport properties and concentration, FCS is also sensitive to changes in the aggregation state of the fluorophore, and use of the method to characterize macromolecular aggregation in biological membranes was proposed (Magde *et al.*, 1978). The ability to measure molecular aggregation states in intact cells is significant because many biochemical reactions, such as signal transduction across the membrane and immune recognition processes, are believed to involve protein oligomerization (Metzger, 1992; Heldin, 1995). However, application of FCS to measurements of membrane

Correspondence: Paul Wiseman. Tel: +1 858 534 0290; fax: +1 858 534 7654; e-mail: pwiseman@ucsd.edu

protein diffusion and aggregation in intact cells proved difficult. The slow diffusion of proteins in biological membranes at 37 °C ($\approx 10^{-10}$ to 10^{-11} cm^2 s^{-1}) entails a relatively long characteristic fluctuation time, making extended measurement times necessary owing to the square root dependence of the FCS signal-to-noise ratio on the number of characteristic fluctuations sampled (Koppel, 1974; Qian, 1990). The long times required to achieve acceptable signal-to-noise ratios were often greater than the available biological time window for measurement on cells which could change their dynamic behaviour or even position over the course of the sampling. To circumvent this problem, Petersen and co-workers introduced an imaging variant of FCS that they called image correlation spectroscopy (ICS) that uses a confocal laser scanning microscope (CLSM) to image fluorescence fluctuations from fluorescent molecules within a cell as a function of space instead of time (Petersen *et al.*, 1993). Spatial autocorrelation analysis of the images yielded information on the molecular concentration and aggregation state (but not dynamics) and this method has been applied to characterize protein aggregation in a number of cellular receptor systems (Wiseman *et al.*, 1997; Brown & Petersen, 1998; Wiseman & Petersen, 1999). To regain sensitivity to molecular dynamics, an extension of ICS was developed that used a CLSM to collect a time series of images from a sample followed by correlation analysis between different images in the time series as well as spatial autocorrelation of the individual images (Srivastava & Petersen, 1996). The method has been used recently to measure the very slow diffusion of receptor clusters in cultured cells (Srivastava & Petersen, 1998). Additionally, a two-colour image cross-correlation spectroscopy (ICCS) variant has been used to demonstrate the colocalization at the plasma membrane of influenza virus haemagglutinin mutant HA + 8 with macromolecular components of coated pits (Brown *et al.*, 1999).

To date, the applications of ICS and ICCS have been restricted to implementations using single photon CLSM collection at relatively slow scan rates. In the current work, we introduce and characterize two-photon excitation ICS and ICCS on a video rate capable microscope. We demonstrate two-photon ICS measurement of diffusion coefficients for fluorescent microspheres of various radii diffusing in water or aqueous sucrose solutions. With the video rate system, we demonstrate that we are able to measure diffusion coefficients that are three orders of magnitude greater than those measurable with ICS on slower CLSM systems. We characterize the use of the video rate two-photon microscope and ICS analysis to measure diffusion over a range of rates as well as the sensitivity of the method to microscopic flow. Furthermore, we show explicitly inherent advantages of the imaging method of sampling and correlation analysis in comparison to standard FCS for obtaining autocorrelation functions with high signal-to-noise in relatively short periods of time. We also present the first demonstration of ICCS using two-photon excitation of multiple fluorophores. We apply two-photon ICCS to characterize the diffusion of microspheres labelled with non-identical fluorophores. Finally, we introduce the use of two-photon ICS to measure lateral mobilities of green fluorescent protein (GFP)/α_5 integrin adhesion receptor fusion proteins on the surface of CHO fibroblast cells.

Materials and methods

Fluorescent microsphere sample preparation

Aqueous solutions were prepared by dissolving sucrose (Sigma Chemical Co., St. Louis, MO) in distilled water. Solutions of 10, 20, 30, 40, 50 and 60% by mass sucrose in water were made. Microsphere suspensions were sonicated for 20 min before use. Microsphere samples were prepared by pipetting 2–5 μL of a suspension of fluorescent microspheres onto a standard microscope slide within the area defined by a plastic spacer. Next, 35–38 μL (for a total volume of 40 μL) of distilled water or aqueous sucrose solution of specified mass percent was pipetted onto the same area of the slide and the suspension was mixed before sealing with a coverslip and nail polish. Samples were made from two types of fluorescent microsphere: carboxylate-modified blue fluorescent microspheres (FluoSpheres, Molecular Probes, Eugene, OR) and multifluorophore fluorescent microspheres (TetraSpeck, Molecular Probes). Blue microspheres having nominal diameters of 0.1, 0.2 and 1.0 μm were used for various samples, whereas only 0.5 μm diameter TetraSpeck microspheres were utilized to prepare multifluorophore samples. Background control samples were also prepared using 40 μL of water or sucrose solution.

Cell culture

The cell line used in these studies was a CHO fibroblast line expressing an α_5 integrin/GFP fusion protein. Professor A. R. Horwitz (Department of Cell Biology, The University of Virginia) and Ms Christina Laukaitis (Department of Cell and Structural Biology, University of Illinois at Urbana-Champaign) developed the cell line and provided us with cells (Knight *et al.*, 2000). The CHO cells were cultured under normal growth conditions in minimum essential medium supplemented with 10% fetal bovine serum, non-essential amino acids and glutamine, as well as 0.5 mg mL^{-1} neomycin (G418) to maintain transfection. Cells were maintained in a humidified, 10% CO$_2$ atmosphere at 37 °C during culturing. Cells used for microscopic observation were plated one or two days before the experiments in culture dishes containing a central glass coverslip.

Two-photon microscopy

Figure 1 shows a schematic of the instrument layout used for these experiments along with a representation of an output image time series. This study employed a Nikon RCM 8000 video rate microscope (Nikon Co., Tokyo, Japan) in inverted configuration, coupled with a Tsunami pulsed femtosecond Ti : sapphire laser (Spectra Physics, Mountain View, CA) pumped by a 5 W Millennium diode laser (Spectra Physics). A fused silica prism sequence is used to pre-compensate for the dispersion of the microscope optics (Müller *et al.*, 1998) and the output wavelength of the laser was tuned to 790 nm. The microscope uses a resonant galvanometer mirror to scan horizontally at the NTSC line scan rate. Point detection is employed using a photomultiplier tube (PMT) with no confocal pinhole, for each of the two detection channels. Various filters were used in combination with a 505 DCLP dichroic mirror (Chroma Technology Co., Brattleboro, VT) for imaging different samples. A D 480/30 nm filter (Chroma Technology Co.) or a 450/40 nm interference filter (OptoSigma, Santa Ana, CA) was used to filter light entering the PMT for channel 1 for all microsphere samples measured. Light entering the second detection channel was filtered with a D 605/55 nm filter (Chroma Technology Co.) for imaging the multi-

labelled TetraSpeck microspheres. All cell samples were imaged at ambient room temperature using a DM 565 dichroic mirror and a D 540/25 nm filter set (Chroma Technology Co.) for the first detection channel. Aspects of the microscope, scan optics, and electronics have been described in more detail previously (Fan *et al.*, 1999).

All image time series were collected using a Nikon $60\times$ water immersion objective lens (NA 1.20). Images having dimensions of 480×512 pixels were collected at a variety of optical zooms: $1\times$, $2\times$ and $4\times$ corresponding to x and y pixel dimensions of 0.228, 0.114 and 0.057 μm/pixel, respectively. Image series were collected with a variety of time delays (0.0333−5 s) between sequential frames depending on the rapidity of the diffusion for a particular sample. Individual image frames for the microsphere sample time series were collected as a rapid (video rate) single scan accumulation irrespective of the time between sequential image frames. Images sampled from the cell preparations were accumulated as averages of between 4 and 32 video rate scans of the basal membrane surface of an individual cell. When images were collected in both detection channels, the maximum frame rate was 15 frames s^{-1} corresponding to the time to sequentially record and write to hard disk two images from the two detectors. The majority of the image time series of the singly labelled microspheres contained 300 sequential image frames. Image series of the multifluorophore TetraSpeck spheres had 150 frames recorded for each detection channel. Time series for the cellular samples were usually collected with 120 image frames.
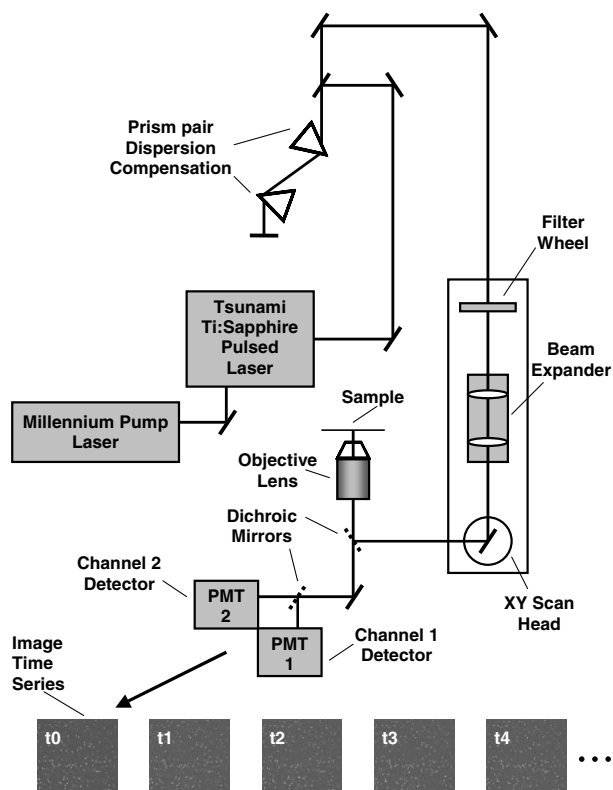
Image autocorrelation and cross-correlation analysis

Correlation calculations for all image time series and nonlinear least squares fitting of the spatial correlation functions were performed on a 333 MHz Sun Ultra 5 workstation (Sun Microsystems, Inc., Palo Alto, CA) using programs written in FORTRAN. Nonlinear least squares fitting to the calculated temporal correlation functions as well as background correction was done on a PC using Sigma Plot for Windows (SPSS, Inc., Chicago IL). The equations used for the calculation and fitting of the normalized intensity fluctuation autocorrelation and cross-correlation functions (both spatial and temporal) are described below (see Theory).

Theory

We present a brief outline of the theory underlying this work and note where complete details can be found in previously published studies. An image time series recorded from detection channel a (where a = 1 or 2) using the two-photon microscope may be considered to be a matrix of fluorescence intensity values stored as a function of pixel

Fig. 1. Diagram of the basic set-up of the lasers and the microscope optics showing beam paths and collected light paths. A representation of an output image time series is also depicted.

location (j, k) and of image number n:

$$\text{Ch } a \text{ Image Series} = i_a(j, k, n), \qquad (1)$$

where j ranges from 1 to 480, k from 1 to 512 and n from 1 to N (the total number of images recorded in the time series). An equivalent representation of this discrete set of intensity data is a matrix of intensities as function of discrete image space and image capture time:

$$\text{Ch } a \text{ Image Series} = i_a(x, y, t), \qquad (2)$$

with

$$\begin{aligned} x &= (j - 1)\delta x \\ y &= (k - 1)\delta y, \\ t &= (n - 1)\delta t \end{aligned} \qquad (3)$$

where δx and δy are lateral spatial pixel dimensions which are equal for square pixels and δt is the time interval between sequential frames. In the following, angular brackets, $< ... >$, represent a spatial averaging. We define a spatial mean intensity for image n in the time series recorded from detection channel a by the following expression:

$$\langle i_a \rangle_n = \frac{1}{480 \cdot 512} \sum_{j=1}^{480} \sum_{k=1}^{512} i_a(j, k, n). \qquad (4)$$

We also define a generalized spatio-temporal correlation function which is a function of spatial lag variables ξ and η and of a temporal lag variable τ for detection channels a and b:

$$r_{ab}(\xi, \eta, \tau) = \frac{\langle \delta i_a(x, y, t) \delta i_b(x, \xi, y + \eta, t + \tau) \rangle}{\langle i_a \rangle_t, \langle i_b \rangle_{t+\tau}}, \qquad (5)$$

where the spatial intensity fluctuations are defined as:

$$\delta i_a(x, y, t) = i_a(x, y, t) - \langle i_a \rangle_t. \qquad (6)$$

In cases where $a = b = 1$ or $a = b = 2$, Eq. (5) defines a normalized intensity fluctuation autocorrelation function for detection channel 1 or 2. When $a = 1$ and $b = 2$, Eq. (5) represents a normalized intensity fluctuation cross-correlation function between the two detection channels. We calculate discrete approximations of the generalized correlation functions defined by Eq. (5) from the finite data record. In the discrete space of the image time series, the spatial lags are simply shifts of $p\delta x$ and $q\delta y$ (p and q are integers) in the orthogonal x and y directions of the original image frame(s). The temporal lag is a whole number multiple of the time interval between image frames, $s\delta t$. We treat the cases for spatial and temporal correlation separately.

Spatial autocorrelation and cross-correlation

For a fixed collection time t, a normalized *spatial* intensity fluctuation autocorrelation function ($a = b = 1$ or 2) or cross-correlation function ($a = 1$ and $b = 2$) may be

defined by evaluating Eq. (5) with zero time lag:

$$r_{ab}(\xi, \eta, 0) = \frac{\langle \delta i_a(x, y, t) \delta i_b(x, \xi, y + \eta, t + \tau) \rangle}{\langle i_a \rangle_t, \langle i_b \rangle_t}. \qquad (7)$$

We calculate the discrete approximation to these correlation functions by Fourier methods and fit them with Gaussian functions by nonlinear least squares methods as has been described previously (Petersen *et al.*, 1993; Srivastava & Petersen, 1996). The generalized Gaussian fit function is represented as follows:

$$r_{ab}(\xi, \eta, 0)_n = g_{ab}(0, 0, 0)_n \exp\left\{\frac{\xi^2 + \eta^2}{\omega_{o\,ab}^2}\right\} + g_{o\,abn}, \qquad (8)$$

where the subscript n denotes spatial correlation functions or fit parameters obtained for a particular image number n (or pair of images for spatial cross-correlation) in the time series. We obtain best fit estimates of the zero spatial lag correlation function amplitude ($g_{ab}(0,0,0)_n$), the e^{-2} beam radius in the focal plane ($\omega_{o\,ab}$), and fitting offset parameter ($g_{o\,abn}$) (Petersen *et al.*, 1993).

Temporal autocorrelation and cross-correlation

A normalized temporal intensity fluctuation autocorrelation function ($a = b = 1$ or 2) or cross-correlation function ($a = 1$ and $b = 2$) may be defined by evaluating Eq. (5) with zero spatial lags:

$$r_{ab}(0, 0, \tau) = \frac{\langle \delta i_a(x, y, t) \delta i_b(x, y, t + \tau) \rangle}{\langle i_a \rangle_t, \langle i_b \rangle_{t+\tau}}. \qquad (9)$$

This function is essentially the temporal persistence of the average spatial correlation between images in the time series that are separated by time delay τ. The discrete approximation to this function is calculated as follows for both the temporal autocorrelation and cross-correlation:

$$\begin{aligned} r_{ab}(0, 0, s) = \frac{1}{N - s} \sum_{c=1}^{N-s} \frac{1}{480 \cdot 512} \\ \times \sum_{j=1}^{480} \sum_{k=1}^{512} \frac{\langle \delta i_a(j, k, c) \delta i_b(j, k, c + s) \rangle}{\langle i_a \rangle_c, \langle i_b \rangle_{c+s}}, \end{aligned} \qquad (10)$$

and this is evaluated with s ranging from 0 to $N - 1$. We calculate these temporal correlation functions directly with Eq. (10) without using Fourier methods, in contrast to Srivastava and Petersen (Srivastava & Petersen, 1996).

For samples containing microspheres undergoing diffusion, we fit the calculated temporal autocorrelation data with functional forms appropriate for a three-dimensional (3D) Gaussian model of the illumination volume (Aragon & Pecora, 1976; Rigler *et al.*, 1993; Schwille *et al.*, 1997):

$$r_{aa}(0, 0, \tau) = g_{aa}(0, 0, 0)\frac{\left(1 + \dfrac{\tau}{\tau_d}\right)}{(1 + (\langle\omega_{o\,aa}\rangle^2/z_{o\,aa}^2)(\tau/\tau_d))^{\frac{1}{2}}} + g_{o\,aa},$$

(11)

where $a = 1$ or $a = 2$. The $g_{aa}(0, 0, 0)$ is the zero time lag best fit amplitude, τ_d is the best fit characteristic diffusion time, and $g_{o\,aa}$ is a fitting offset parameter that accounts for cases where the correlation function does not decay to zero at longer lag times. The e^{-2} beam radii, $\langle\omega_{o\,aa}\rangle$ and $z_{o\,aa}$, are fixed as constants for the fitting. The $\langle\omega_{o\,aa}\rangle$ value is the mean lateral radius obtained by averaging the $\omega_{o\,aa}$ values obtained in the fitting of the individual spatial autocorrelation functions for each image in the series. The $z_{o\,aa}$ value is the beam radius in the axial direction of the focus and is obtained from optical sectioning point-spread function measurements of standard fluorescent dyes. The temporal cross-correlation functions were fit with the same functional form as Eq. (11), but the beam radii constants were replaced with dual channel effective radii:

$$\langle\omega_{o12}\rangle = \left\{\frac{\langle\omega_{o11}\rangle^2 + \langle\omega_{o22}\rangle^2}{2}\right\}^{\frac{1}{2}}, \quad z_{o12} = \left\{\frac{z_{o11}^2 + z_{o22}^2}{2}\right\}^{\frac{1}{2}}$$

(12)

as was done previously for dual colour FCS (Schwille *et al.*, 1997). Time series exhibiting microscopic flow were only recorded for the singly labelled microspheres. Temporal autocorrelation functions calculated for these 'flow' samples were fit with the appropriate functional form (Magde *et al.*, 1978):

$$r_{11}(0, 0, \tau) = g_{11}(0, 0, 0)\exp\left\{-\left(\frac{v\tau}{\langle\omega_{o\,11}\rangle}\right)^2\right\}, \quad (13)$$

where v is the best fit mean flow velocity and $g_{11}(0, 0, 0)$ and $\langle\omega_{o\,11}\rangle$ are fit parameters as described above.

We fit the calculated temporal autocorrelation data from the cellular samples with the functional form appropriate for diffusion within a two-dimensional (2D) area illuminated by a focused laser beam with Gaussian intensity profile in the xy focal plane (Srivastava & Petersen, 1996):

$$r_{11}(0, 0, \tau) = g_{11}(0, 0, 0)\exp\left(1 + \frac{\tau}{\tau_d}\right)^{-1} + g_{o11}, \quad (14)$$

where the symbols used are the same as described for Eq. (11) above.

Diffusion coefficients were calculated using the best fit lateral beam radius and the characteristic diffusion time (Elson & Magde, 1974):

$$D_{exp} = \frac{\langle\omega_{o\,ab}\rangle^2}{4\tau_d}. \quad (15)$$

Note that ω_o is the effective two-photon beam radius and not the radius for the fundamental wavelength. For some samples, the theoretical diffusion coefficient was calculated for comparison purposes using the Stokes–Einstein relationship:

$$D_{theory} = \frac{kT}{6\pi\eta r}, \quad (16)$$

where k is Boltzmann's constant, T is absolute temperature, η is the viscosity of the solvent, and r is the microsphere radius.

Results

Figure 2 shows typical images of fluorescent microsphere samples selected from image time series collected using the RCM 8000 two-photon video rate microscope. In Fig. 2A we present an image of 0.2 μm diameter blue fluorescent microspheres suspended in water. In Figs 2(B) and (C) we show images simultaneously sampled in two different wavelength detection channels of 0.56 μm diameter multi-labeled microspheres suspended in a 60% by mass sucrose aqueous solution.

In Fig. 3 we present examples of temporal autocorrelation functions calculated from image time series recorded for samples of 0.2 μm blue fluorescent microspheres undergoing random diffusion in water (Fig. 3A) or unidirectional flow of 1 μm spheres in a 50% by mass sucrose aqueous solution (Fig. 3B). The data points were calculated from the image time series using Eq. (10), and the functions of best fit, which are depicted as solid lines, were determined by fitting to Eq. (11) for the diffusing microspheres or to Eq. (13) for the flow sample. The τ_d value obtained from the fitting of the curve in Fig. 3A was 0.0229 s, which yields a diffusion coefficient of 2.2×10^{-8} cm^2 s^{-1} when calculated using Eq. (15) and the mean lateral beam radius for this experiment. This value of D matches that predicted by the Stokes–Einstein relationship (Eq. 16) for spheres of 0.2 μm diameter in water at the recording temperature of 292.2 K. A best fit flow velocity of $v = 1.6 \pm 0.2$ μm s^{-1} was obtained from the fit to the data in Fig. 3(B). This corresponds well to an estimate of 1.9 ± 0.2 μm s^{-1} made by tracking five individual microspheres as a function of time over 60 frames and calculating the mean velocity.

In Fig. 4, we show results for the two-photon ICS measurement of diffusion coefficients for 0.2 μm blue fluorescent microspheres suspended in aqueous sucrose solutions of varying concentrations. The experimental data are plotted as a function of the theoretically predicted diffusion coefficient calculated using Eq. (16) and data for the viscosity of sucrose solutions (taking dilution effects into account), measured temperature, and the mean sphere radius. Each point represents the mean of the autocorrelation results for five individual time series measurements on a given sample and the error bars depict the standard error of the mean (SEM). Individual autocorrelation functions were calculated from all 300 images in a time series, but only the first 60 time-lag points were included for
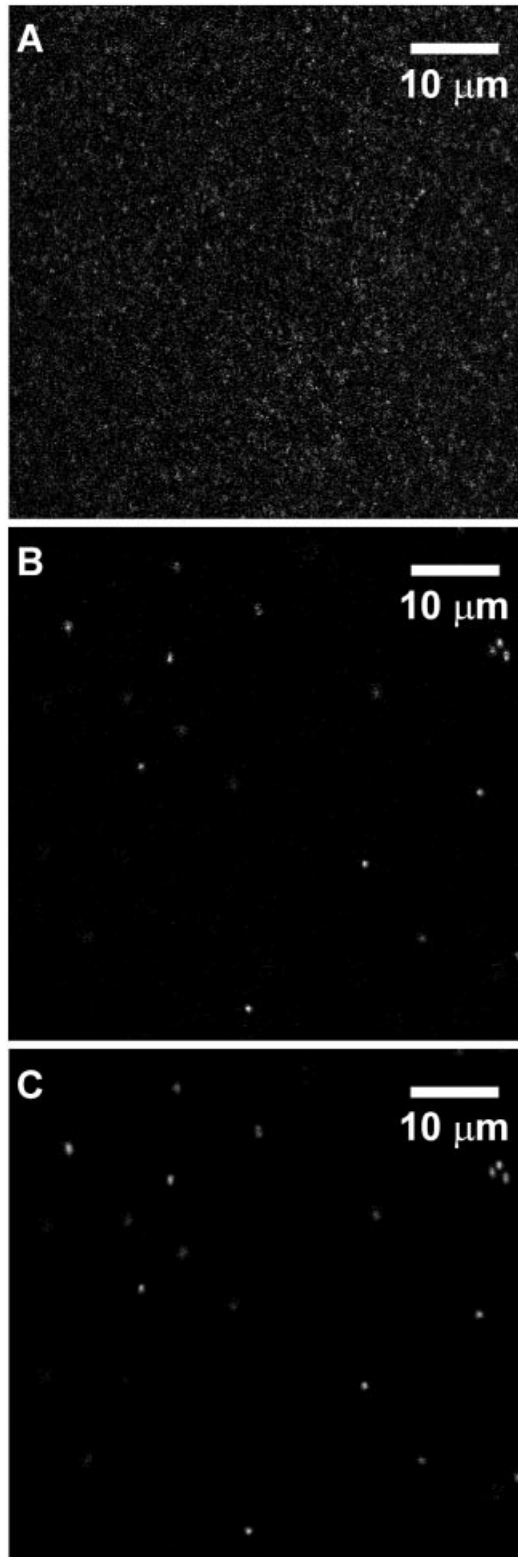
determination of the function of best fit. A linear regression was determined from the data and is shown in Fig. 4. The regression line has a slope of 0.97 for these data. The calculated average diffusion coefficients had a relative uncertainty of between 5 and 6% for this experiment.

In Fig. 5 we present data that illustrate the effects that finite image sampling time has on the quality of the calculated autocorrelation functions. The autocorrelation functions depicted in the figure were all calculated from the same image time series, but differ in the total number of images (i.e. time lags) included in the calculation via Eq. (10). The sample imaged was a microscope slide with 0.2 μm blue fluorescent microspheres suspended in water at 19 °C. The original image series consists of 300 images sampled at video rate (30 f/s) using the two-photon microscope. Temporal autocorrelation functions calculated from the first 30, 150 and all 300 image frames (corresponding to maximum time lags of 1, 5 and 10 s, respectively) are plotted with a logarithmic scale for the temporal lag axis. The inset graph shows the same autocorrelation functions graphed with an added offset constant that was used to separate the plots in the vertical direction. We fit these data sets using Eq. (11) to examine the convergence of the autocorrelation function fitting for data with variable time sampling. The best fit characteristic diffusion time, τ_d, was 0.019 s, 0.018 s and 0.016 s for the respective 300, 150 and 30 image data sets.

Additionally, we calculated time autocorrelation functions for a single pixel location for all time points in an image series. Figure 6 shows the results for the calculation of two single-pixel time autocorrelation functions. The temporal autocorrelation function shown in Fig. 6A was calculated from the intensity time series recorded at pixel position (200, 200) for all 300 images in the same series that was used for the calculation of the correlation functions depicted in Fig. 5. For comparison purposes, we also calculated a time autocorrelation function from the intensity time record for a single-pixel location in an image series that was recorded for twice as long (20 s) from a sample containing 1 μm blue fluorescent microspheres in water. This is presented in Fig. 6(B).

In Fig. 7 we show results from two-photon ICCS analysis

Fig. 2. Images of fluorescent microspheres suspended in aqueous solution. Images were selected from time series collected using two-photon excitation and the RCM 8000 video rate microscope. (A) Image of 0.2 μm diameter blue fluorescent microspheres in water collected in the first detection channel through a 450/40 nm interference filter. (B) Image of 0.56 μm diameter multilabelled fluorescent microspheres suspended in a 60% by mass sucrose aqueous solution as collected in the first detection channel through a 450/40 nm interference filter. (C) Image of the same fluorescent microsphere sample as in (B), but collected simultaneously in the second detection channel through a 605/55 nm filter.
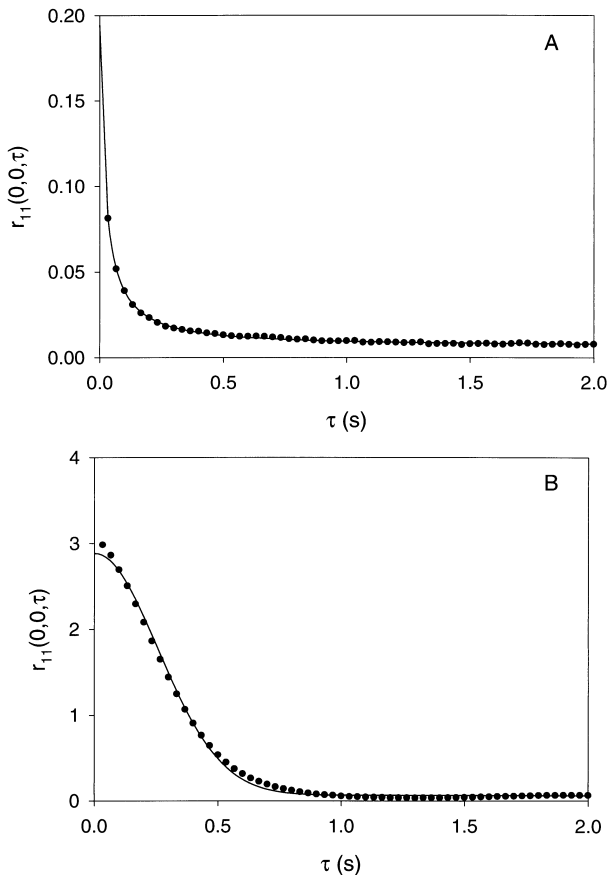
Fig. 3. Normalized temporal intensity fluctuation autocorrelation function data and functions of best fit calculated from two-photon video microscopy image time series of blue fluorescent microspheres in aqueous sucrose solutions. (A) Temporal autocorrelation function data and best fit function calculated for a video rate image time series of randomly diffusing of 0.2 μm diameter blue fluorescent microspheres in water. (B) Temporal autocorrelation data and function of best fit determined from a video rate image time series of flowing 1.0 μm diameter blue fluorescent microspheres suspended in a 50% by mass sucrose in water solution. Autocorrelation function data are represented by (●) while the functions of best fit are shown by (—).

of image time series measured in two detection channels for 0.56 μm multilabelled microspheres suspended in an aqueous sucrose solution. Figure 7 depicts the temporal autocorrelation functions for the two detection channels as calculated using Eq. (10): $r_{11}(0,0,\tau)$ and $r_{22}(0,0,\tau)$, respectively. A plot of the temporal cross-correlation function, $r_{12}(0,0,\tau)$, is also shown. Non-linear least squares fitting was performed using Eq. (11) and diffusion coefficients calculated from the best fit results using Eq. (15). The diffusion coefficients determined for the calculated correlation functions were identical within a 5% experimental uncertainty. The best fit amplitudes of the correlation functions were also indistinguishable within experimental error.
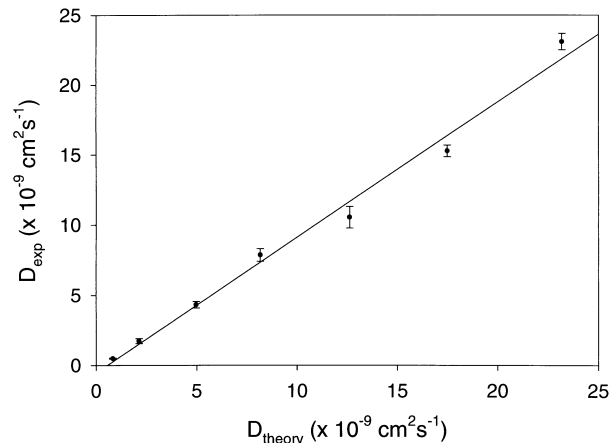

Fig. 4. A plot of experimentally measured diffusion coefficient vs. theoretical diffusion coefficient as predicted by the Stokes–Einstein relationship (Eq. 16) along with the linear regression line for these data. Each experimental data point represents a mean of five ICS measurements made on a single sample and the error bars represent the standard error of the mean (SEM). The samples are 0.2 μm diameter blue fluorescent microspheres suspended in aqueous sucrose solutions having different solute concentrations and the image series were collected at 20 $\pm$ 2 °C. The slope of the regression line is 0.97 and r^2 equals 0.989 for this fit.

We present results from the application of two-photon ICS for studies on living cells in Fig. 8. Using the two-photon RCM8000, we imaged fluorescence from GFP/α_5 integrin adhesion protein constructs on the basal surface of CHO fibroblasts that were maintained in growth medium at room temperature on the microscope stage. Figure 8A depicts an image of the GFP/integrin receptor distribution on the basal membrane of a single CHO fibroblast. We imaged as a function of time from the basal surface of individual cells and calculated the temporal intensity fluctuation autocorrelation function from the image series via Eq. (10). An example of a temporal autocorrelation function determined from a cellular image time series is shown in Fig. 8(B) along with its function of best fit (fitting model Eq. 14). The τ_d value obtained from the best fit curve in Fig. 8(B) was 217 s and from which a diffusion coefficient of 4.8 $\times$ 10^{-12} cm^2 s^{-1} was calculated. To confirm the applicability of the 2D diffusion model, we plotted the reciprocal of the temporal autocorrelation function value as a function of lag time and performed a linear regression (Thompson, 1991). The plot of $r_{11}(0,0,\tau)^{-1}$ vs. τ was linear with a squared correlation coefficient of 0.998 (plot not shown).

Discussion

The results presented in Fig. 3 demonstrate that the two-photon ICS method that we have developed is sensitive to both microscopic diffusion and flow. We have shown that we can accurately measure both diffusion coefficients and
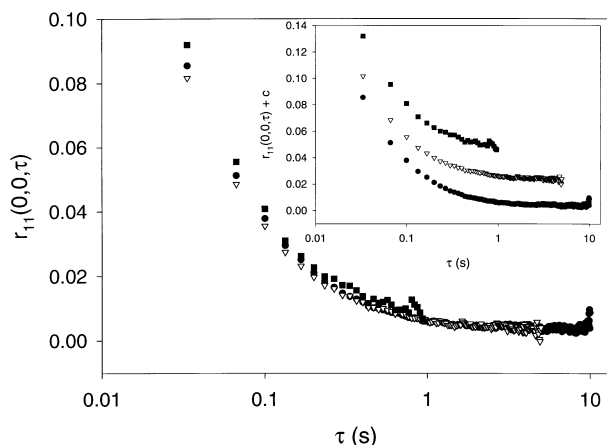
Fig. 5. A plot of temporal intensity fluctuation autocorrelation functions calculated from a single measured image time series incorporating variable numbers of images into the function calculation. The two-photon microscopy image time series was collected from a sample of 0.2 μm diameter blue fluorescent microspheres suspended in water at an ambient temperature of 19 °C. ■ represents the autocorrelation function calculated from the initial 30 images in the time series. ▽ shows the temporal correlation function calculated from the first 150 images in the time series, and ● represents the autocorrelation function calculated using all 300 images in the time series. The inset graph depicts the same autocorrelation functions plotted with an offset constant c for the purpose of separating the data in the vertical direction for visual comparison purposes. The offset c was 0.04, 0.02 and 0 for the 30, 150 and 300 data point correlation functions, respectively. A logarithmic temporal lag axis is used to emphasize the functional decay trends at short time lags.

flow velocities by autocorrelation analysis of image time series collected using a video rate capable two-photon imaging system. We also demonstrated accurate measurement of diffusion coefficients of fluorescent microspheres in aqueous solutions having variable viscosity (Fig. 4). We were able to measure diffusion coefficients as large as 10^{-8} cm^2 s^{-1}, which is three orders of magnitude larger than those reported for single-photon CLSM time correlation measurements with ICS (Srivastava & Petersen, 1996). This time scale makes ICS measurement of more rapid diffusive events in biological membranes possible. Phospholipid diffusion, which occurs at such rates, could be measured by video rate two-photon ICS after labelling of membrane lipid molecules with fluorescent microspheres. Diffusion at faster time scale, which can occur intracellularly, is not measurable by the video rate ICS that we have introduced, but can be measured by standard FCS techniques (Berland et al., 1995; Brock & Jovin, 1998). We are also sensitive to diffusion at slower rates and our control measurements on immobilized fluorescent microspheres indicate a detection limit on the order of 10^{-13} cm^2 s^{-1} (data not shown). Thus, we retain the full sensitivity to

diffusion rates characteristic of proteins in biological membranes that was reported for single photon ICS (Srivastava & Petersen, 1996), but are also able to characterize faster transport processes. Our two-photon approach to ICS and ICCS should provide additional advantages for applications to measurements on living cells because multiphoton fluorescence microscopy is considered to be less damaging to living specimens than single photon fluorescence imaging (Denk et al., 1990).

We report an experimental uncertainty of 5–6% for the measurement of diffusion coefficients for the 0.2 μm diameter fluorescent microspheres via two-photon ICS. This is a smaller uncertainty than the 10–20% reported for previous single photon ICS measurements of diffusion coefficients for larger (0.88 μm) diameter microspheres (Srivastava & Petersen, 1996). This could be due to increased spatial sampling as well as increased averaging due to the collection of more data in the image time series in the current study.

The approach we chose for calculation of the temporal autocorrelation functions for two-photon ICS differs somewhat from that reported previously by Srivastava & Petersen (1996). They obtained the temporal autocorrelation function by calculating the normalized spatial cross-correlation between different images in a single time series by Fourier methods and then obtaining the zero spatial lags value for each of these functions. We decided against this approach because it involves the calculation of all spatial lags for all time lags. These data are not used anyway. For time series collected at video rate, the number of images can become large and the approach of determining every possible spatial cross-correlation between all images in the time series becomes computationally prohibitive. Our approach simply calculates the correlation explicitly for zero spatial lags as a function of the time lags in the image series. We also differ from Srivastava and Petersen in our fitting of a 3D Gaussian model to the calculated temporal correlation functions instead of a 2D Gaussian model. We found that we did not obtain convergence to the theoretical diffusion coefficients when we employed the 2D model (data not shown), but did with the 3D Gaussian model. Recent single- and two-photon FCS experiments have also found reasonable experimental agreement by fitting time correlation functions with a 3D Gaussian model (Schwille et al., 1999).

Our results show that one of the inherent advantages of the imaging approach to correlation analysis is the ability to rapidly obtain temporal correlation functions with high signal-to-noise. The rapid convergence of the temporal autocorrelation functions can be seen in Fig. 5, where reasonable signal-to-noise was achieved even for image series collected for only 1 s. The high signal-to-noise of the autocorrelation functions is due to the inherent spatial averaging of the ICS approach. Examination of Fig. 6 shows that autocorrelation functions calculated for a single pixel
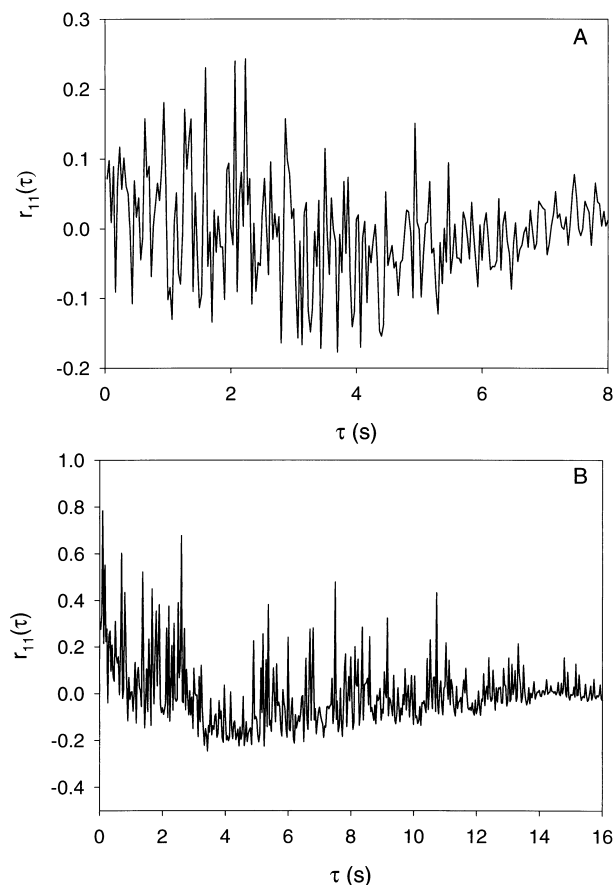
Fig. 6. Plots of temporal intensity fluctuation autocorrelation functions calculated for single pixel locations in image time series collected from samples of blue fluorescent microspheres suspended in water. (A) Single pixel temporal autocorrelation function calculated for pixel position (200, 200) for all 300 images (10 s) in the same image time series as was used to calculated the correlation functions depicted in Fig. 3. (B) Single pixel temporal autocorrelation function calculated for one pixel position using all 600 images (20 s) of a time series collected from a sample of 1.0 μm diameter microspheres in water at an ambient temperature of 19 °C. Solid lines connect the calculated discrete autocorrelation data points and best fit functions are not shown.

time series show very high noise for comparable length of measurement. Even the single pixel time autocorrelation function for the larger (hence brighter) 1 μm microspheres for a 20-s time series has excessive noise and the functional decay can barely be discerned. For comparable signal-to-noise, a single spatial channel measurement of diffusion at these orders of magnitude (i.e. an FCS type measurement) would typically require integration times of 10 min or longer. This advantage of the imaging approach is especially important for measurements of transport properties in systems where the characteristic diffusion rate is relatively slow, such as for proteins in biological membranes, as has been suggested before (Srivastava & Petersen, 1996). Our

current work provides the first systematic demonstration of how the spatial averaging achieved through imaging can allow for greatly reduced observation times for the measurement of temporal correlation functions. For ICS measurements on biological membranes, however, there can be cell samples that exhibit inhomogeneous spatial distributions of macromolecules. In such cases it can be necessary to sacrifice in the spatial averaging by performing the ICS analysis over smaller image subsections and collecting the time series for longer periods of time. This approach involves the balancing of experimental variables of spatial and temporal sampling space, yet it still retains the benefits of image correlation, but on a smaller scale.

We have also presented results of the first demonstration of two-photon excitation image cross-correlation spectroscopy (ICCS) for the measurement of microscopic transport properties. An examination of Fig. 7 shows that the auto-correlation and cross-correlation functions for the two wavelength channels match both in amplitude and decay time (and hence diffusion coefficient), which is expected for the samples containing multilabelled fluorescent micro-spheres. This approach to fluorescence cross-correlation measurements offers certain advantages over single-photon excitation schemes that have been employed previously (Schwille *et al.*, 1997; Brown *et al.*, 1999). A single excitation volume is defined by the focus of the laser beam in the two-photon approach, which can efficiently excite multiple fluorophores, due to the broad bandwidths intrinsic to ultrashort pulses. For two-photon fluorescence microscopy without pinholes, the correlation observation volume for multiple fluorophores is fully determined by the spatial extent of the focus of the excitation beam. For single-photon two-colour FCS, careful alignment and overlap of multiple laser beams is required or conversely for non-overlapping beams, interpretation of the experimental data becomes far more complicated (Schwille *et al.*, 1997). Our method, using two-photon excitation of multiple fluoro-phores by tightly focused ultrashort laser pulses, is much easier to set up experimentally.

Our initial application of the two-photon ICS method to measurements on living cells demonstrates that temporal autocorrelation functions can be measured with high signal-to-noise on cells expressing a GFP/fusion protein, as can been seen in Fig. 8(B). We measured slow diffusion of the GFP/α_5 integrin receptor constructs within the basal membrane at room temperature on different cells in two different samples. The diffusion coefficients measured ranged between 4.5 and 6.0×10^{-12} cm^2 s^{-1}. A plot of the reciprocal of the temporal autocorrelation function amplitude vs. lag time should be linear for 2D diffusion (Thompson, 1991). We tested this by plotting the autocorrelation data in this way and confirmed linear behaviour as expected for diffusion of the receptors within the planar basal membrane.
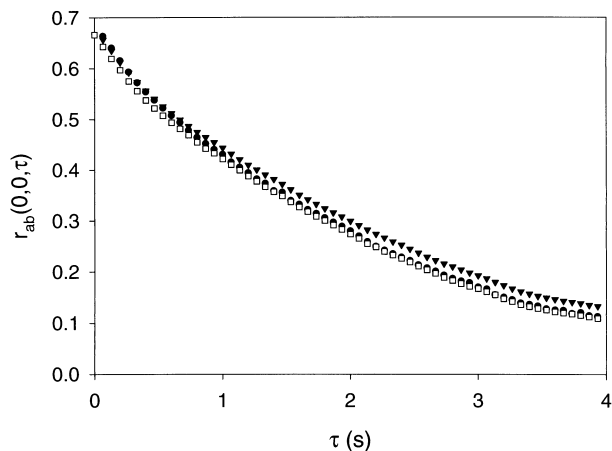
Fig. 7. Plots of temporal auto- and cross-correlation functions calculated from image time series collected in two detection channels for non-identical fluorophores simultaneously excited by two-photon absorption of light from a single incident pulsed laser. The sample consisted of multilabelled 0.56 μm diameter fluorescent microspheres suspended in a 60% by mass aqueous sucrose solution at an ambient temperature of 20 °C. ● depicts the temporal autocorrelation function, $r_{11}(0,0,\tau)$, calculated for the first detection channel (480 nm), and ▼ shows the autocorrelation function, $r_{22}(0,0,\tau)$, calculated from the image series for the second detection channel (605 nm). □ represents the temporal cross-correlation function, $r_{12}(0,0,\tau)$, calculated between image series of the first and second detection channels.

The data collection is ultimately limited by photobleaching of the GFP fluorophore within the cells. However, we were able to detect the loss of signal in a time series because the fitting of the spatial autocorrelation functions would no longer converge when the fluorescence had attenuated beyond a minimum threshold level. The total number of images that could be scanned in a time series, before breakdown in the spatial fitting occurred, varied from cell to cell. In one time series, the spatial fitting breakdown occurred early after collection of 39 image frames with each image being an accumulation of 16 scans (i.e. 624 total scans). However, for other cells, we collected time series of 120 image frames with each image being an accumulation of 32 scans (i.e. 3840 total scans) with no breakdown of the spatial autocorrelation fitting. This variation in the total number of meaningful images that could be collected in a time series probably arises from differences in expression levels of the GFP/α_5 integrin receptors between cells.

We were able to measure temporal autocorrelation functions for image time series where individual frames were collected as an accumulation of four scans. Greater numbers of scans per image (16 or more) were generally required to measure the spatial correlation functions with reasonable precision. These initial data suggest that we can perform time autocorrelation experiments for transport
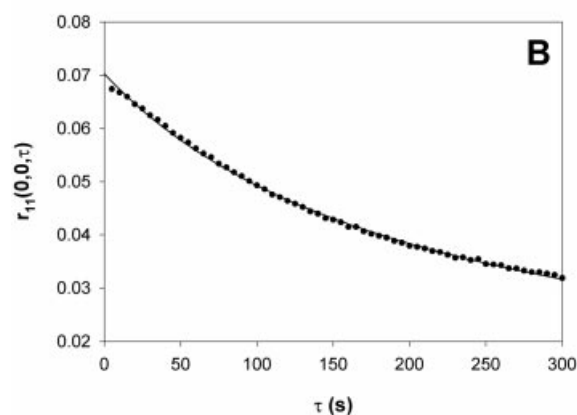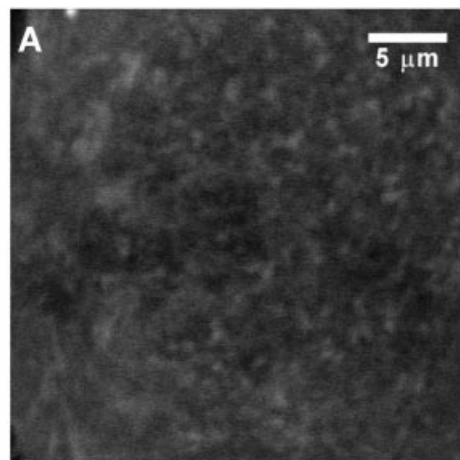

Fig. 8. Two-photon imaging and ICS of a living cell. (A) Image of GFP/α_5 integrin adhesion receptor constructs on the basal membrane of a CHO fibroblast cell. The sample, CHO fibroblasts maintained in growth medium at room temperature on the stage of the RCM 8000 microscope, was imaged using two-photon excitation. The image was collected as an average of 256 scans (8.5 s) in the first detection channel through a 540/25 nm filter. (B) Normalized temporal intensity fluctuation autocorrelation function data (●) and function of best fit (—) calculated from a two-photon microscope image time series of basal GFP/α_5 integrin adhesion receptor constructs on a single cell. A total of 120 images were collected in the time series, with each image being an average of 32 scans (1.1 s) and with a time step of 5 s between sequential images. Stage temperature was 20 °C.

studies using the RCM8000 microscope with a time step resolution of 0.13 s. Spatial autocorrelation amplitude studies as a function of time for monitoring molecular aggregation are restricted to image time steps of 0.5 s due to the need to accumulate sufficient numbers of scans per image frame. We note that for these initial cellular measurements we did not use photobleaching inhibitors.

We have introduced variants of ICS and ICCS that utilize two-photon excitation and a fast video rate capable imaging microscope. We have demonstrated accurate measurement

of diffusion coefficients and flow at higher signal-to-noise, and for microscopic particles diffusing up to three orders of magnitude faster than previously reported for CLSM based ICS. We have shown systematically the benefits of the spatial image correlation approach for measurement of transport properties in systems where observation time is limited. We have also reported the use of simple two-photon excitation of multiple fluorophores to perform an image cross-correlation measurement of microscopic transport. In the current work we have focused on the measurement of transport properties in dynamic systems via two-photon ICS and ICCS. The amplitude information that is accessible through correlation type measurements is also of interest, especially in applications in cellular systems where it can be sensitive to the aggregation of biomolecules (Berland *et al.*, 1996; Wiseman & Petersen, 1999). We are continuing investigations with the two-photon ICS and ICCS methods to study their applicability for measuring molecular aggregation phenomena in living cells.

Acknowledgements

References

Aragon, S.R. & Pecora, R. (1976) Fluorescence correlation spectroscopy as a probe of molecular dynamics. *J. Chem. Phys.* **64**, 1791–1803.

Berland, K.M., So, P.T.C., Chen, Y., Mantulin, W.M. & Gratton, E. (1996) Scanning two-photon fluctuation correlation spectroscopy: particle counting measurements for detection of molecular aggregation. *Biophys. J.* **71**, 410–420.

Berland, K.M., So, P.T. & Gratton, E. (1995) Two-photon fluorescence correlation spectroscopy: method and application to the intracellular environment. *Biophys. J.* **68**, 694–701.

Brock, R. & Jovin, T.M. (1998) Fluorescence correlation microscopy (FCM) − Fluorescence correlation spectroscopy (FCS) taken into the cell. *Cell. Mol. Biol.* **44**, 847–856.

Brown, C.M. & Petersen, N.O. (1998) An image correlation analysis of the distribution of clathrin associated adaptor protein (AP-2) at the plasma membrane. *J. Cell Sci.* **111** (27), 1–281.

Brown, C.M., Roth, M.G., Henis, Y.I. & Petersen, N.O. (1999) An internalization-component influenza Hemagglutinin mutant causes the redistribution of AP-2 to existing coated pits and is colocalized with AP-2 in clathrin free clusters. *Biochemistry,* **38**, 15166–15173.

Denk, W., Strickler, J.H. & Webb, W.W. (1990) 2-Photon laser scanning fluorescence microscopy. *Science,* **248**, 73–76.

Elson, E.L. & Magde, D. (1974) Fluorescence correlation spectroscopy. 1. Conceptual basis and theory. *Biopolymers,* **13**, 1–27.

Fan, G.Y., Fujisaki, H., Miyawaki, A., Tsay, R.X., Tsien, R.X. & Ellisman, M.H. (1999) Videorate scanning two-photon excitation fluorescence microscopy and ratio imaging with cameleons. *Biophys. J.* **76**, 2412–2420.

Heldin, C. & 11. (1995) Dimerization of cell surface receptors in signal transduction. *Cell,* **80**, 213223.

Knight, B., Laukaitis, C., Akhtar, N., Hotchin, N.A., Edlund, M. & Horwitz, A.R. (2000) Visualizing cell migration *in situ. Curr. Biol,* **10**, 576–585.

Koppel, D.E. (1974) Statistical accuracy in fluorescence correlation spectroscopy. *Phys. Rev. A,* **10**, 1938–1945.

Magde, D., Elson, E. & Webb, W.W. (1972) Thermodynamic fluctuations in a reacting system: measurement by fluorescence correlation spectroscopy. *Phys. Rev. Lett. (USA),* **29**, 705708.

Magde, D., Elson, E.L. & Webb, W.W. (1974) Fluorescence correlation spectroscopy. H. An experimental realization. *Biopolymers,* **13**, 29–61.

Magde, D., Webb, W.W. & Elson, E.L. (1978) Fluorescence correlation spectroscopy. 111. Uniform translation and laminar flow. *Biopolymers,* **17**, 361–376.

Metzger, H. (1992) Transmembrane signaling: the joy of aggregation. *J. Immunol.* **149**, 14771487.

Müller, M., Squier, J., Wolleschensky, R., Simon, U. & Brakenhoff, G.J. (1998) Dispersion precompensation of 15 femtosecond optical pulses for high-numerical-aperture objectives. *J. Microsc.* **191**, 141–150.

Petersen, N.O., Höddelius, P.L., Wiseman, P.W., Seger, O. & Magnusson, K.E. (1993) Quantitation of membrane receptor distributions by image correlation spectroscopy: concept and application. *Biophys. J.* **65**, 1135–1146.

Qian, H. (1990) On the statistics of fluorescence correlation spectroscopy. *Biophys. Chem.* **38**, 49–57.

Rigler, R., Mets, U., Widengren, J. & Kask, P. (1993) Fluorescence correlation spectroscopy with high count rate and low background: analysis; of translational diffusion. *Eur. Biophys. J.* **22**, 169–175.

Schwille, R., Haupts, U., Maiti, S. & Webb, W.W. (1999) Molecular dynamics in living cells observed by fluorescence correlation spectroscopy with one- and two-photon excitation. *Biophys. J.* **77**, 2251–2265.

Schwille, P., Meyer-Almes, F.J. & Rigler, R. (1997) Dual-color fluorescence cross-correlation spectroscopy for multicomponent diffusional analysis in solution [see comments]. *Biophys. J.* **72**, 1878–1886.

Srivastava, M. & Petersen, N.O. (1996) Image cross-correlation

spectroscopy: a new experimental biophysical approach to measurement of slow diffusion of fluorescent molecules. *Meth. Cell Sci.* **18**, 47–54.

Srivastava, M. & Petersen, N.O. (1998) Diffusion of transferrin receptor clusters. *Biophys. Chem.* **75**, 201–211.

Thompson, N.L. (1991) Fluorescence correlation spectroscopy. *Topics in Fluorescence Spectroscopy*, **Vol. 1**: Techniques (ed. by J. R. Lakowicz), pp. 337–378. Plenum Press, New York.

Wiseman, P.W., Höddelius, P., Petersen, N.O. & Magnusson, K.E. (1997) Aggregation of PIDGF-beta receptors in human skin fibroblasts: characterization by image correlation spectroscopy (ICS). *FEBS Lett.* **401**, 43–48.

Wiseman, P.W. & Petersen, N.O. (1999) Image correlation spectroscopy. II. Optimization for ultrasensitive detection of preexisting platelet-derived growth factor-beta receptor oligomers on intact cells. *Biophys. J.* **76**, 963–977.